Chemical and Process Engineering 2021, 42 (3), 275–289
DOI: 10.24425/cpe.2021.138931

Solution blow spun poly-L-lactic acid/ceramic fibrous composites for bone implant applications

Michał Wojasiński[1*], Tomasz Ciach[1,2]

[1]Warsaw University of Technology, Faculty of Chemical and Process Engineering, Waryńskiego 1, 00-645 Warsaw, Poland

[2]Warsaw University of Technology, Centre for Advanced Materials and Technologies CEZAMAT, Poleczki 19, 02-822 Warsaw, Poland

Every bone implant to work correctly after implantation needs to integrate with the surrounding bone. To enhance such a process, called osseointegration, various techniques of implant surface modification emerged. One of the approaches is based on the deposition of nano- and submicron materials on the implant surface. This paper presents a solution blow spinning process for producing poly-L-lactic acid (PLLA)/ceramic fibrous composites designed to be deposited directly onto orthopaedic implants prior to implantation to increase osseointegration. We produced plain PLLA fibrous materials for comparison, and fibrous composite materials with β-tricalcium phosphate (βTCP), hydroxyapatite nanoparticles (nHAp) and hydroxyapatite nanoparticles modified with lecithin (nHAp-LE). We performed the structural analysis of produced materials with scanning electron microscopy, gravimetric determination of porosity, and water contact angle measurement. We also used infrared spectroscopy, Alizarin Red S staining, and cytotoxicity evaluation to conclude that PLLA/nHAp-LE composite material shows the most promising properties to be applied as surface modification of bone implants. To visualise fibrous composite deposition on implants, we used two models: titanium plate and stainless-steel bolt. Thus, we showed that the solution blow spun materials can be used for surface modification of orthopaedic implants.

Keywords: solution blow spinning, composite fibres, submicron fibres, nanofibres, poly-L-lactic acid, ceramic particles, bone implants

1. INTRODUCTION

A perfect bone implant, especially for the treatment of large bone defects, needs to meet several criteria, which can be divided into three major groups: 1) structural features, 2) composition, and 3) biological features. Structural features of bone-implant materials, especially those for tissue engineering applications, focus primarily on porosity and pore's interconnectivity and topography and shape of the implant itself (Roseti et al., 2017). At the same time, the composition should resemble the composition of natural bone – a composite material of collagenous polymer and calcium phosphate ceramic serving as a scaffolding material for bone cells (Sharma and Elisseeff, 2004). Both structural features and composition affect the mechanical properties of the implant. What is more, they affect the biological response of the recipient of

* Corresponding author, e-mail: michal.wojasinski@pw.edu.pl

the implant after the surgery. In general, bone implant materials should exhibit suitable osseointegration properties (for long term implants) without causing unwanted effects on the surrounding tissue resulting in inflammation and foreign body response. For more than three decades, the most used implant material has been titanium and titanium alloys. They are generally biocompatible with bone tissue and exhibit superior mechanical stability and strength. However, they differ from the natural bone with some physical properties, like thermal conductivity and expansion, Young modulus. Additionally, in many cases, the osseointegration of the titanium or titanium alloy implant can be limited, depending on an implant's shape and surface properties (Carlsson et al., 1986). Several approaches based on the increase of surface roughness emerged to increase the rate of the osseointegration of titanium-based bone implants. Those approaches include surface roughening, ceramic coating, synthetic coating, natural coating, and peptide coating (Civantos et al., 2017). The synthetic coating includes but is not limited to, deposition of fibrous structures on the bone-implant surface (Li et al., 2007; Ravichandran et al., 2012).

Electrospinning (ES), a method of producing fibres with sizes ranging from a few nanometres to a few micrometres (Reneker and Yarin, 2008), appeared as an effective way of depositing fibrous structures on collector surfaces. What is more, electrospinning allows the production of composite fibrous structures consisting of hydroxyapatite nanoparticles (nHAp) or other osteoactive materials, like β-tricalcium phosphate (βTCP) (Jang et al., 2009; Ravichandran et al., 2012; Tammaro et al., 2014). However, deposition of different fibrous materials on the surface of implants using ES remains difficult since the source of the driving force in the process is a high voltage applied between a nozzle and a collector. Moreover, the collecting material needs to be conductive (Behrens et al., 2014). In the 2000s, the solution blow spinning (SBS) process emerged, proposed independently by François et al. (2009); Medeiros et al. (2009); and Zhang et al. (2009). In general, SBS applies shear drag forces of the high-speed air stream to the polymer solution droplet to form fibrous materials on the collector. Although the design of the coaxial nozzle system for SBS may pose some difficulties compared to electrospinning, the simplicity of the rest of the SBS system overcomes this drawback. What is more, the efficiency of SBS can be at least ten times higher compared to electrospinning (Huang et al., 2019), and SBS is much less susceptible to spinning liquid qualities like electrical conductivity and surface tension (Kopeć et al., 2020). Capabilities of the SBS process mirror those of ES in terms of the composition of fibrous materials. SBS allows the production of nano- and submicrometric composite fibres with reinforcements in the form of nanoparticles. Examples of such composite fibrous materials produced by SBS include photocatalytic poly-L-lactic acid (PLLA) and titanium oxide (TiO_2) fibrous composite (Costa et al., 2016), antimicrobial materials based on silver nanoparticles reinforcing poly(dimethylsiloxane) (PDMS) fibres (Ferreira et al., 2019), other antimicrobial silver (Ag) and titanium oxide (TiO_2) composites based on poly(vinylpyrrolidone) (PVP) (Bonan et al., 2019), and polystyrene fibres reinforced with metal-organic frameworks (MOFs) (Deneff and Walton, 2019). Moreover, research groups reported the production of fibrous scaffolds with the addition of osteoactive substances like nHAp (Abdal-hay et al., 2013; Abdal-hay et al., 2015), bioactive glass (Medeiros et al., 2021). Apart from the low cost and simplicity of the production system, SBS main advantage remains in producing fibrous structures on various surfaces. Those surfaces include classic metallic collectors in the form of cylinders or plates, but also the skin (Medeiros et al., 2009), metallic implants, wooden parts, rubber, and threaded metals and ceramics (Abdal-Hay et al., 2016; Tutak et al., 2013). What is more, Behrens et al. (2014) used fibres produced with an SBS system in a sterile environment to stop the bleeding in the operating room (on pig model).

Capabilities of the SBS process allowing the production of composite fibrous structures with fibre size in the submicron scale and the possibility to collect such fibres on various surfaces inspired present research. We aimed to develop a composite fibrous material to be deposited directly on the bone-implant surface using solution blow spinning. We used PLLA as a primary material for producing composite fibrous structures using osteoactive substances as reinforcement. Osteoactive materials included commercially available βTCP and nHAp powders and self-synthesised nHAp modified with lecithin (nHAp-LE) (Latocha et al., 2018). First, we characterised the physical properties of composite materials using scanning electron

microscopy, water contact angle measurement, Fourier transform infrared spectroscopy and Alizarin Red S (ARS) staining, and biological properties by XTT cytotoxicity assay. Then, we demonstrated the possibility to deposit PLLA/nHAp-LE submicron fibrous material on the surface of titanium plate and steel bolt.

2. MATERIALS AND METHODS

2.1. Composite fibre production

A schematic representation of polymer solution and polymer/ceramic solution preparation is depicted in Figure 1. Poly-L-lactic acid (PLLA, $M_w \geq 200$ kDa, BiomerL9000, Germany), a biodegradable polyester, was used as the primary material for plain and composite fibre preparation. Based on our prior research, the mixture of acetone and chloroform (3:1 v/v ratio, both Chempur, Poland) was used as a good polymer solvent for solution blow spinning (Tomecka et al., 2017). The polymer solution was prepared in 6%w/w concentration by 24 h mixing using a magnetic stirrer. As prepared, PLLA solution was used in the solution blow spinning (SBS) process to produce plain PLLA nanofibrous material. Ceramic particles used as reinforcement in composite nanofibres consisted of β-tricalcium phosphate (βTCP, SigmaAldrich, Germany), commercially available hydroxyapatite nanoparticles (nHAp, SigmaAldrich, Germany), and self-synthesised hydroxyapatite nanoparticles modified with lecithin (nHAp-LE, produced in the continuous reactor according to Latocha et al. (2018)). Ceramic particles were dispersed in a polymer solution using ultrasounds for 5 minutes. The final polymer concentration of 6%w/w and the mass ratio of ceramic particles of 1:3 to the polymer was achieved (25%w/w of ceramic in the final composite fibrous structure), and such mixtures of polymer and ceramic particles in the mixture of chloroform and acetone were used for solution blow spinning. The codification of the materials is as follows: PLLA – plain poly-L-lactic acid fibres; PLLA/βTCP – poly-L-lactic acid fibres reinforced with βTCP; PLLA/nHAp

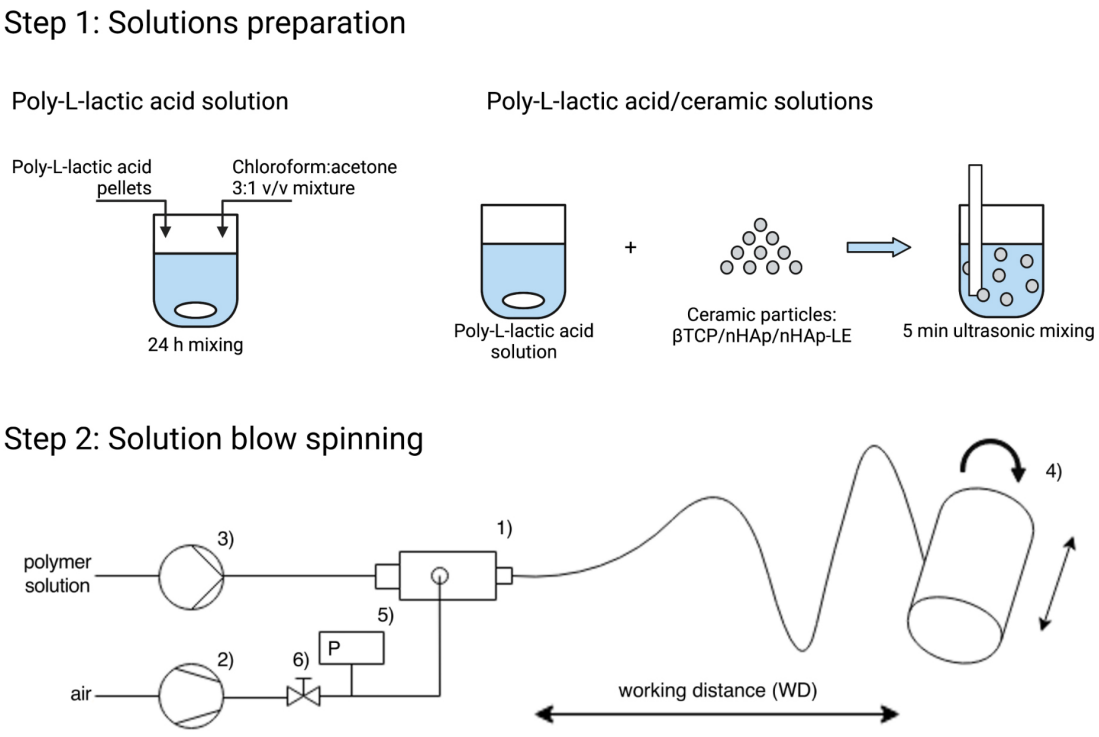

Fig. 1. Step 1: Schematic representation of poly-L-lactic acid solution preparation for plain fibres and composite production. Step 2: Solution blow spinning (SBS) setup schematic representation: 1) concentric nozzle system, 2) air pump, 3) injection pump, 4) rotating collector, 5) barometer, 6) valve. Created with https://biorender.com/

– poly-L-lactic acid fibres reinforced with commercially available nHAp particles; PLLA/nHAp-LE – poly-L-lactic acid fibres reinforced with nHAp particles modified with lecithin.

Polymer solution and polymer/ceramic suspensions were subjected to the spinning process using the SBS system presented in Figure 1 (described in detail in Wojasiński et al. (2014)). Briefly, the polymer solution or polymer/ceramic solution was supplied through the inner nozzle in the concentric nozzle system (Fig. 1-1) of the SBS system with a feed rate of 30 mL/h. At the same time, the air stream was supplied through the outer nozzle of the concentric nozzle system with an air pressure of 1 bar. Due to the rapid decompression of the air, the air velocity increased, and the shear-drag interactions between the air stream and the surface of polymer solution (or polymer/ceramic solution) caused the formation of the jet. From the apex of the jet, the fibrous filament thread originated. The air stream elongated the thread and evaporated the solvents, and the resulting fibre flown through the working distance between the nozzle system and the collector and was collected on the surface of the rotating cylinder – collector (Fig. 1-4). The spinning process was conducted for 20 minutes (10 mL of polymer or polymer/ceramic solution) to prepare the material with a uniform thickness of about 200 μm. The resulting mat was cut open and pealed from the surface of the collector for further analysis.

2.2. Scanning electron microscopy

A scanning electron microscope (SEM, SU8320, Hitachi, Japan) visualised ceramic particles and visualised and measured SBS's fibrous structures. Before SEM investigations, ceramic powder samples were prepared as follows. First, a few micrograms of the powder were spread on the surface of the conductive carbon tape. Then, the sample was sputtered with a 10 nm layer of Au:Pd alloy (80:20 mass ratio) using Q150T Sputter (Quorum, UK). For fibrous materials, the 5 mm × 5 mm sample was cut from the fibrous mat and glued to the carbon tape. Then, the surface of the sample was sputtered as ceramic samples. The Fiji software (v2.1.0/1.53c) was used to measure fibre diameter and pore size in fibrous samples (Schindelin et al. (2012)). Fibre and pore sizes are presented as size distribution with mean ± standard deviation (SD, n = 100) and as box-whisker plots, where whiskers represent minimum and maximum, while the box represents 25th and 75th percentile, and the line inside the box represents the median of the size distribution. The "plus" sign inside the box represents the mean value of the fibre size and pore size in the distribution.

2.3. Porosity measurement

The porosity of the fibrous materials was measured using the gravimetric method (Tomecka et al., 2017; Tutak et al., 2013) using the following formula (1):

$$\varepsilon \ [\%] = 1 - \frac{\rho_s}{\rho_{\text{material}}} \times 100\% \tag{1}$$

where ρ_s is the density of the fibrous sample calculated using the following formula (2):

$$\rho_s = \frac{m_s}{\delta A} \tag{2}$$

The sample thickness, δ, was measured using SEM (n = 25), while ρ_{material} is the bulk density of the material used in the spinning process. For the plain PLLA fibres, ρ_{material} = 1250 kg/m^3 (ρ_{PLLA}) (Balakrishnan et al., 2012), and for the composite materials, ρ_{material} was calculated using the following formula (3):

$$\rho_{\text{material}} = f_{\text{PLLA}}\rho_{\text{PLLA}} + (1 - f_{\text{PLLA}})\,\rho_{\text{ceramic}} \tag{3}$$

where f_{PLLA} is the volume fraction of the polymer in the composite, and ρ_{ceramic} is the density of the ceramic material in the composite, for βTCP – ρ_{ceramic} = 3140 kg/m3 ($\rho_{\beta\,\text{TCP}}$), and for both nHAp and nHAp-LE – ρ_{ceramic} = 3100 kg/m^3 (ρ_{nHAp}, $\rho_{\text{nHAp-LE}}$) (McEvoy, 1992; Lewis, 1997). Porosity, ε, was reported as mean ± SD (n = 5).

2.4. Water contact angle measurement

Measurement of the wettability property of the PLLA and PLLA/ceramic fibrous materials was conducted using DSA 100 goniometer (Krüss, Germany). For each type of material, the 5 µL drop of distilled water was placed on the surface of the fibrous materials, and the water contact angle (WCA) was measured for 10 seconds with one frame per second (1 fps) frequency. The measurement was performed in triplicates. Therefore, water contact angle results are presented as mean ± SD (n = 30).

2.5. Fourier transform infrared spectroscopy

The availability of the ceramic particles at the surface of composite fibrous materials, compared to plain PLLA fibres, was determined by Fourier transform infrared (FTIR) spectroscopy using a Nicolet™ 6700 spectrometer (Thermo Fisher Scientific USA). Spectra were detected in attenuated total reflection (ATR) mode and analysed with the OMNIC 8.3 software. Spectra were recorded for at least three randomly selected spots for each sample of plain and composite materials. One characteristic spectrum for each tested material was selected for presentation.

2.6. Alizarin-Red S staining

Availability of the calcium moieties at the surface of composite materials, compared to the plain PLLA fibres was determined using Alizarin Red S (ARS, SigmaAldrich, Germany) staining. The protocol was adapted from Gregory et al. (2004) and Tutak et al. (2013). First, each material (n = 3) was incubated with 1 mL of 40 mM (pH 4.1) solution of ARS in distilled water for 1 h. Then, each material was washed with distilled water three times, with 5 minutes of shaking each time. After the washing step, ARS was extracted from the materials using 1 mL of 10%w/v solution of cetylpyridinium chloride monohydrate (Sigma-Aldrich, Germany) in distilled water. Extracts were collected and transferred to a 96-well plate for absorbance measurement (405 nm) using Epoch (BioTek, USA) microplate reader. Results are presented as mean optical density (OD) ± SD (n = 6).

2.7. Cytotoxicity evaluation

Cytotoxicity of produced fibrous materials, plain PLLA fibres and PLLA/ceramic composites was determined using XTT (sodium 3′-[1-[(phenylamino)-carbony]-3,4-tetrazolium]-bis(4-methoxy-6-nitro)benzene-sulfonic acid hydrate) test on extracts, adapted from the ISO 10993-5:2009. For the cytotoxicity evaluation, the MG63 human osteosarcoma cell line (SigmaAldrich, Germany) was used. After sterilisation with 70% ethanol solution (1 mL, for 5 minutes) and washing with phosphate-buffered saline (PBS, two times, 1 mL, 5 minutes), fibrous scaffold made of PLLA, PLLA/βTCP, PLLA/nHAp, and PLLA/nHAp-LE was immobilised in a 24-well plate and covered with 1 mL of extraction medium for 24, 48 and 72 h for obtaining scaffold extracts. Dulbecco's Modified Eagle Medium (DMEM, Thermo Fisher Scientific, USA) supplemented with 10% fetal bovine serum (FBS, Thermo Fisher Scientific, USA) and antibiotics (100 U/mL penicillin, 100 mg/mL streptomycin, Thermo Fisher Scientific, USA) was used as extraction medium and maintenance medium for cells. Additionally, a sterile solution of 0.1% Tween 80 in supplemented DMEM was prepared and incubated in the same periods as a positive control. Supplemented DMEM was used as a negative control. MG63 cell line was inoculated in 96-well plates in a concentration of 10^5 cells/mL and 100 µL of culture medium per each well and incubated for 24 h at 37 °C, 5% CO_2. After this time, the DMEM was replaced by extracts. Cells after 24 h of incubation with extracts were washed twice with 100 µL of PBS. Then, 100 µL of DMEM, without phenol red and supplementation, and 50 µL of XTT solution with coupling reagent (The Cell Proliferation Kit II [XTT], Roche, Germany)

was added to each culture well, and plates were incubated for 4 h. After the XTT was reduced to formazan by living cells, the assay medium (100 µL from each well) was transferred to a new 96-well plate, and the absorbance at 475 nm was measured in an Epoch microplate reader. The relative cell viability was defined as the absorbance ratio from the sample to the absorbance measured for negative control and represented as a mean value ± standard deviation (n = 8).

2.8. Statistical analysis

The normality of distributions of fibre size, pore size, porosity, water contact angle, ARS staining, and cytotoxicity results were tested using the Kolmogorov-Smirnov normality test with Dallal-Wilkinson-Lilliefor P value (p = 0.05). The difference among the mean fibre sizes, mean pore sizes, mean porosities, mean water contact angles of analysed materials was tested in the Kruskal–Wallis test (p = 0.05), with post hoc nonparametric Dunn's test for multiple comparisons. The difference among the mean OD value in the ARS staining test, the difference among mean values of the analysed materials' cytotoxic properties were tested in one-way ANOVA (p = 0.05) with post hoc Tukey's test for multiple comparisons.

3. RESULTS

3.1. Fibrous composite structural properties

The morphology of ceramic particles, βTCP, nHAp, and nHAp-LE, used as reinforcement in produced PLLA/ceramic fibrous materials, is shown in Figures 2a to 2c. The largest particles occurred in βTCP powder, with the size within the microscale range (from about 1 to 10 µm, Fig. 2a). Both nHAp and nHAp-LE powders consisted of agglomerated nanoparticles. In nHAp commercially available from SigmaAldrich, the producer specifies the mean particle size below 150 nm (Fig. 2b). For nHAp-LE, Latocha et al. (2018) reported the size of basic particles that build the agglomerates to range from about 20 to 30 nm (Fig. 2c). Comparing Figures 2b and 2c, one can identify that agglomeration of nHAp and nHAp-LE particles is similar, but nHAp-LE particles created more densely packed particles that can be identified as aggregates.

Figures 2d to 2g show the morphological features of plain PLLA fibres and PLLA/ceramic composites. In all the investigated materials, the morphology and size of the fibres within the material remains in the submicron range, without an apparent increase of the fibre size for composites, compared to plain PLLA fibres. However, the uniformity of the reinforcement distribution within PLLA/ceramic composites differs depending on the type of reinforcement. For βTCP and nHAp-LE, agglomerates and/or aggregates of ceramic powders are visible in SEM images (Fig. 2e and Fig. 2g). Nevertheless, in the case of nHAp (commercially available), nanoparticles are more uniformly distributed.

Results of digital analysis of the SEM images of fibrous materials allowed the determination of the fibre size distribution (Fig. 3a) and pore size distribution (Fig. 3b). What was not visible in SEM images, the mean fibre size of composite materials increased, compared to plain PLLA. Plain PLLA fibres exhibited a mean fibre size of 216 ± 99 nm (median: 190 nm), while for composite fibrous materials, mean fibre size was: for PLLA/βTCP – 251 ± 114 nm (median: 220 nm), for PLLA/nHAp – 243 ± 87 nm (median: 230 nm), and PLLA/nHAp-LE – 275 ± 119 nm (median: 251 nm). The difference between the means was statistically significant (Fig. 3a). The change of mean pore size did not result in the increase of the mean fibre size for all the investigated materials (Fig. 3b). Plain PLLA fibrous material exhibited mean pore size of 4.49 ± 2.08 µm (median: 4.10 µm), while for composite fibrous materials, mean pore size was: for PLLA/βTCP – 4.81 ± 2.53 µm (median: 4.26 µm), for PLLA/nHAp – 5.08 ± 2.43 µm (median: 4.54 µm), and for PLLA/nHAp-LE – 4.72 ± 2.25 µm (median: 4.073 µm).

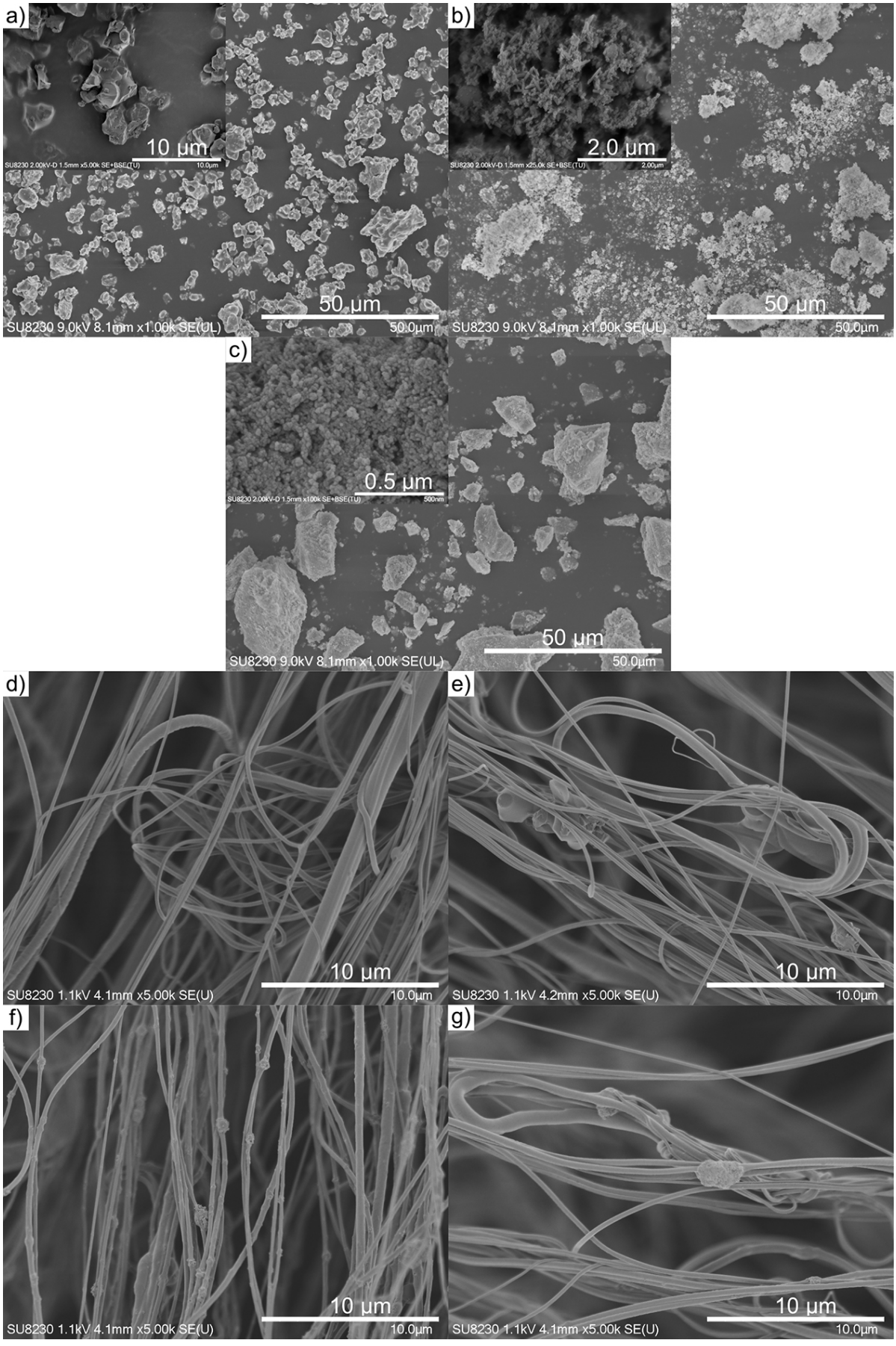

Fig. 2. SEM images of a) βTCP ceramic particles, b) nHAp ceramic particles, c) nHAp-LE ceramic particles, d) plain PLLA fibres, e) composite PLLA/βTCP fibres, f) composite PLLA/nHAp fibres, g) composite PLLA/nHAp-LE fibres

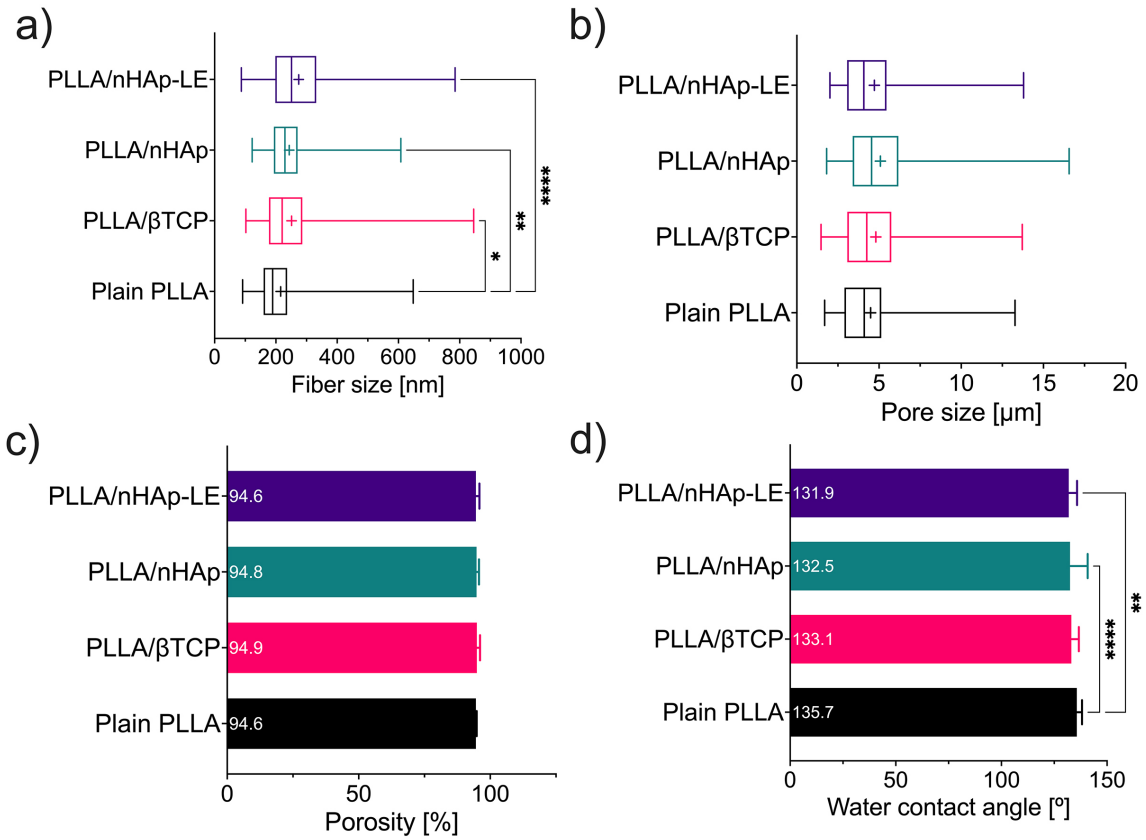

Fig. 3. a) fibre size distributions, b) pore size distributions, c) porosity, and d) water contact angle for PLLA, PLLA/βTCP, PLLA/nHAp, and PLLA/nHAp-LE. Asterisks denote samples significantly different with * $0.01 < p < 0.05$, ** $0.001 < p < 0.01$, **** $p < 0.0001$

The addition of ceramic particles to the polymer solution for producing composite fibrous materials in the SBS system resulted in no porosity change compared to the plain PLLA fibrous materials (Fig. 3c). All tested materials showed porosity of about 95%, which indicates that PLLA/ceramic composite materials from SBS might serve as a promising scaffold for cell ingrowth.

Another feature of every biomaterial that affects the interactions of cells with the scaffold is WCA. The presence of ceramic particles in composite materials reduced slightly, compared to plain PLLA, WCA, but only in the case of nHAp and nHAp-LE materials. The mean WCA for PLLA fibrous materials was 135.7 ± 2.5°, while PLLA/nHAp – 132.5 ± 8.4° and PLLA/nHAp-LE – 131.9 ± 4.0°. The difference between PLLA and PLLA/nHAp and PLLA and PLLA/nHAp-LE was statistically significant (Fig. 3d). In the case of PLLA/βTCP, WCA was 133.1 ± 3.6°.

3.2. Ceramics availability

Production of polymer/composite fibrous materials using the SBS process allowed a relatively uniform distribution of ceramic particles within the fibrous structure (see Fig. 2). However, microscopic methods allow to analyse only one spot at a time. FTIR-ATR measurement revealed IR spectra showing distinct groups from polymer and ceramic within the larger area of the samples (Fig. 4a). In all investigated composite materials, there were peaks characteristic for IR spectra of calcium phosphates coming from the PO_4^{3-} group (for wavenumbers of about 560, 600, 960 and 1020 cm^{-1}). Additionally, the polymer characteristic groups of polyesters appeared for wavenumbers of about 1760 to 1780 cm^{-1}.

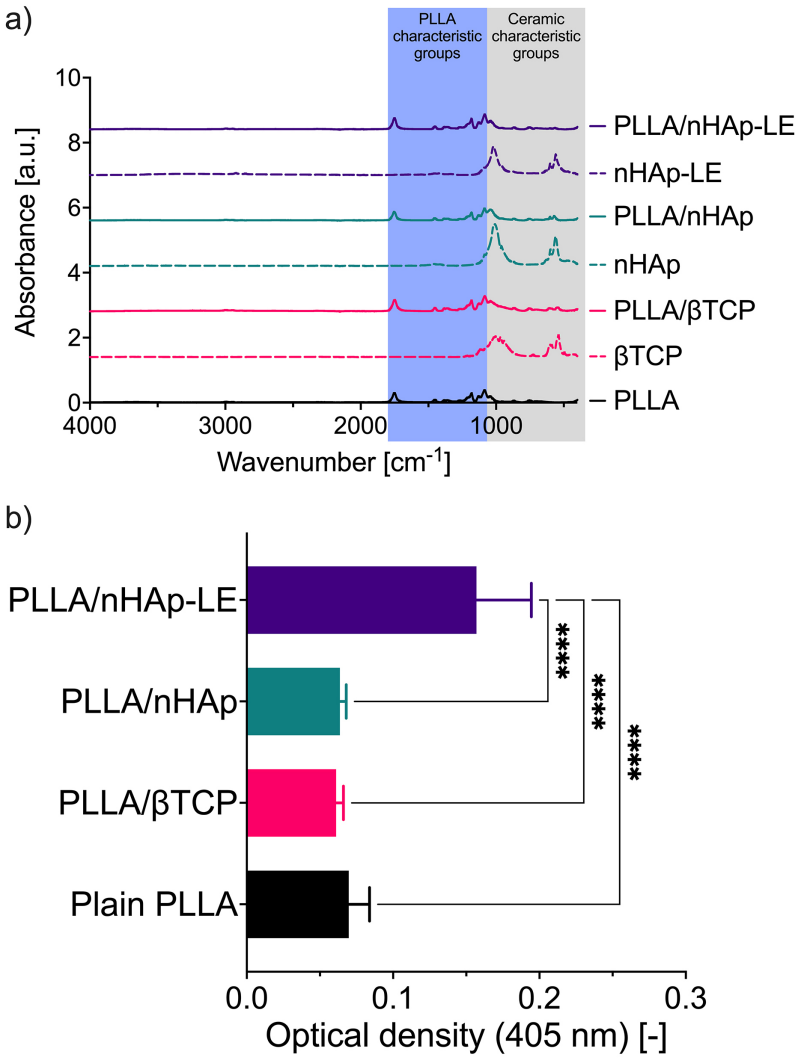

Fig. 4. a) FTIR-ATR spectra for plain PLLA, PLLA/βTCP, PLLA/nHAp, PLLA/nHAp-LE composite materials, and reinforcing ceramics βTCP, nHAp, and nHAp-LE, b) Alizarin Red S extract absorbance expressed in optical density (OD) for 405 nm. Asterisks denote a sample significantly different from the others with (****) $p < 0.0001$

The availability of the ceramic reinforcement on the surface of the composite materials was investigated also using Alizarin Red S staining. Results presented in Figure 4b show that most of the ceramic material was available for the staining compound in PLLA/nHAp-LE composites (mean OD = 0.157 ± 0.038). Other investigated materials: PLLA (mean OD = 0.070 ± 0.015), PLLA/βTCP (mean OD = 0.061 ± 0.06), and PLLA/nHAp (mean OD = 0.064 ± 0.005), had OD significantly lower than PLLA/nHAp-LE.

3.3. Fibrous composite cytotoxicity

Cytotoxic properties of plain PLLA fibrous material and PLLA/ceramic fibrous composites were investigated by XTT assay (Fig. 5). Cell viability, determined as a percentage of living cells compared to the negative control (NC), in extract-based XTT assay showed no cytotoxic properties – cell viability below 70% – of all investigated materials after 24-, 48- and 72-hour extraction (material incubation in extraction medium). After the extraction was performed over three days, PLLA/βTCP and PLLA/nHAp showed significantly lower cell viability than the NC (Fig. 5). For the same period, the PLLA/nHAp-LE material extract resulted in slightly elevated cell viability.

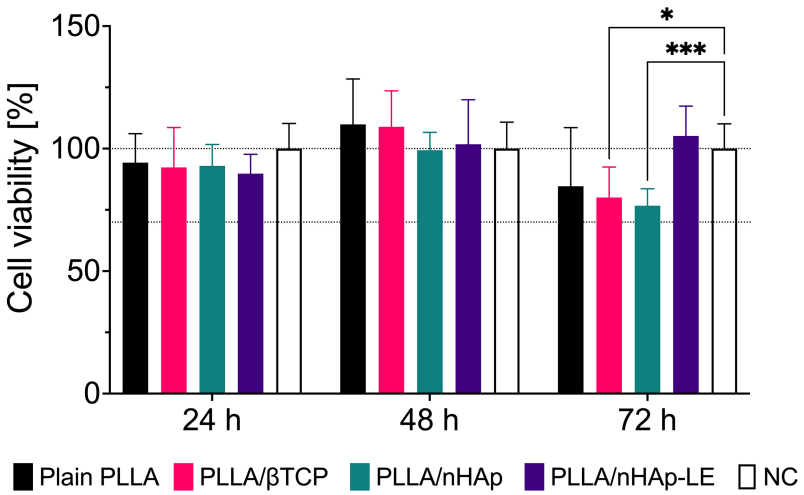

Fig. 5. XTT cytotoxicity test results of extracts obtained in 24, 48 and 72 h of incubation in extracting media for plain PLLA, PLLA/βTCP, PLLA/nHAp, and PLLA/nHAp-LE composite materials (including negative control – NC). Dotted lines indicate a non-cytotoxic range (from 70 to 100%). Asterisks denote samples significantly different with (*) $0.01 < p < 0.05$, (***) $0.0001 < p < 0.001$

3.4. Application of composite fibres for titanium implants

To determine the possibility of applying solution blow spinning of polymer/ceramic materials as a method of implant coating, the deposition of PLLA/nHAp-LE fibres was performed on the surface of titanium plate (Fig. 6a) and steel bolt (Fig. 6b). In both cases, a uniform layer of the material covered the surface.

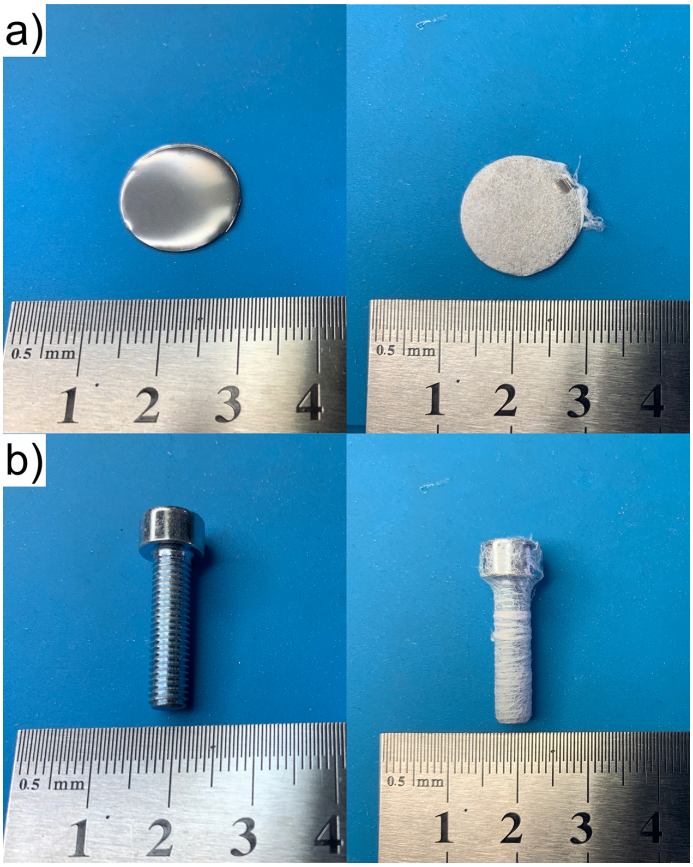

Fig. 6. Examples of a) titanium plate and b) stainless steel screw covered with composite PLLA/nHAp-LE fibrous layer

4. DISCUSSION

The application of the SBS process to produce various composite fibrous structures was already discussed in the introduction. However, in bone-implant applications, only composite structures produced with osteoactive compounds like βTCP, nHAp or bioglass as reinforcement are vital. Abdal-hay et al. (2013) demonstrated that using PLLA as a primary material, they could use hydroxyapatite nanoparticles in the amount of reinforcement in the composite corresponding to about 10-15%w/w. In another paper, Abdal-hay et al. (2015) showed explicitly that the amount of nHAp within their composite was as high as 10%w/w. The present paper showed that the SBS process allowed mixing the polymer and ceramic particles within the working solution with a ceramic concentration of up to 25%w/w. What is more, the structural properties of the composite fibrous materials we produced using PLLA/ceramic solutions were similar to the properties of composite fibrous materials previously reported by other research groups (Abday-hay et al., 2013; Abdal-hay et al., 2015; Medeiros et al. 2021). In this case, the structural properties generally unaffected by the addition of osteocative reinforcements include pore size and porosity. However, the mean fibre size of composite materials depends on the concentration of the reinforcement in the fibrous composites, according to Abday-hay et al. (2015). There is no direct comparison of different types of reinforcement influence on the mean fibre size in the literature. However, in the present paper, the increase of the mean fibre size is independent of the type of reinforcement, and this increase of the mean fibre size depends only on the presence of the reinforcement itself. Moreover, the closeness of the reinforcement particles to the fibre surface is probably the leading cause of fibre size increase. Researchers demonstrated in the literature that the main parameter causing the increase of the fibre size in the SBS process is the polymer concentration in the solution. The increase of polymer concertation usually increases the apparent viscosity of the solution (Daristotle et al., 2016). Similarly, in the case presented here, the observed effect of the fibre size increase in SBS of composite fibres might come from the increase of apparent viscosity of the polymer/ceramic solutions. The change of the other processing parameters in SBS – polymer solution feed rate and gas pressure – has an insignificant influence on the quality of the product, as we reported in our previous study (Wojasiński et al., 2014).

In general, hydrophilic materials require no additional treatment before cell seeding in tissue engineering applications. What is more, high wettability or superhydrophilicity are considered essential factors speeding up the cell's adhesion to the biomaterial's surface and proliferation within the biomaterial (Kopeć et al., 2020). Composite materials showing the reinforcement on their surface (see Fig. 2) might exhibit reduced WCA compared to plain PLLA fibrous materials due to higher affinity to the water of βTCP and nHAp. In the presented case, only the addition of nHAp and nHAp-LE reduced the WCA of fibrous composite. However, the effect of reduced WCA values was significantly lower than expected, compared to the changes reported by Abdal-hay et al. (2013). Since the reduction of WCA in the presented case was low, we suggest an application of pre-treatment of all investigated materials before any experiments involving direct cell seeding on the surface of the scaffolds.

Although the reinforcement particles did not affect the wetting property of the investigated composite fibrous materials produced using the SBS process, the availability of the ceramic on the surface of the composite was evident in FTIR-ATR and ARS staining experiments. However, in the case of calcium deposits availability for the ARS staining compound, only PLLA/nHAp-LE composites showed promising results, while other materials only exhibited calcium phosphate characteristic groups in IR spectra. Also, after 24 and 48 hours of extracting periods, designed to leach any cytotoxic compounds or the excess of the calcium ions from the fibrous composites, there was no significant difference amongst the tested materials. However, after 72 hours, even though they were still within the range specified for non-cytotoxic materials, PLLA/βTCP and PLLA/nHAp extract rendered a significantly lower response than negative control in the XTT assay based on ISO 10993-5 standard. On the other hand, plain PLLA showed a slightly lower response than the negative control, but the composite PLLA/nHAp-LE fibrous scaffold

leached no cytotoxic compounds and remained at a similar level of response as the negative control in the XTT assay.

Up until now, Tutak et al. (2013) tested direct deposition of plain solution blow spun fibres on various non-living surfaces like metal, wood and ceramic. Later, Abdal-hay et al. (2016) deposited composite PLLA/nHAp fibres on the surface of magnesium alloy intended as a material for temporary bone implant. Based on the above mentioned results, we decided to test the applicability of the PLLA/nHAp-LE solution for the SBS process designed to deposit the fibres onto metallic model surfaces – a titanium plate and a steel bolt. The results of such experiments are promising. The sample of titanium plate and stainless-steel bolt were covered totally by the fibrous structure of PLLA/nHAp-LE material. Hence, the solution blow spun materials can be used for surface modification of bone implants. However, extensive tests for the bioactivity of presented composites should be done before prospective animal and human trials.

5. CONCLUSIONS

SBS allows to produce nano- and submicron fibrous composite materials composed of βTCP, nHAp or nHAp-LE intended for the surface modification of titanium orthopaedic implants. The resulting submicron composite fibrous materials exhibit structural properties almost unchanged compared to plain PLLA submicron fibrous mats. The ultrasound used to mix the polymer and ceramic particles in the solution and subsequent spinning allows uniform distribution of ceramic reinforcement within the composite. However, only the addition of lecithin-modified hydroxyapatite nanoparticles to the composite (PLLA/nHAp-LE) resulted in the highest availability of calcium on the surface of the composite amongst tested materials. The submicron composite fibres, regardless of the reinforcing material, are non-cytotoxic and can be easily deposited on various surfaces, including plates or threads – types of surfaces typical in orthopaedic prostheses and fixing materials (fixing plates and screws). All the mentioned properties of the resulting fibrous composite material and ability of fibre deposition on various surfaces render the solution blow spinning a suitable process for surface modification of orthopaedic materials.

SYMBOLS

A	sample area, m^2
ARS	Alizarin Red S
DMEM	Dulbecco's Modified Eagle Medium
ES	electrospinning
f	volume fraction, –
FBS	foetal bovine serum
fps	frames per second
FTIR-ATR	Fourier transform infrared spectroscopy in attenuated total reflectance mode
IR	infrared
ISO	International Organization for Standardisation
MOF	metal-organic framework
NC	negative control
nHAp	hydroxyapatite nanoparticles
nHAp-LE	hydroxyapatite nanoparticles modified with lecithin
OD	optical density
PBS	phosphate-buffered saline
PDMS	poly(dimethylsiloxane)

PLLA	poly-L-lactic acid
PVP	poly(vinylpyrrolidone)
SBS	solution blow spinning
SD	standard deviation
SEM	scanning electron microscope
WCA	water contact angle
XTT	cytotoxicity assay based on sodium 3′-[1-[(phenylamino)-carbony]-3,4-tetrazolium]-bis(4-methoxy-6-nitro)benzene-sulfonic acid hydrate
βTCP	β-tricalcium phosphate

Greek symbols

δ	sample thickness, m
ε	porosity, %
ρ	density, kg/m^3

Subscripts

ceramic	a general term for ceramic materials
material	a general term for bulk density of materials
nHAp	hydroxyapatite nanoparticles
nHAp-LE	hydroxyapatite nanoparticles modified with lecithin
PLLA	poly-L-lactic acid
s	sample
βTCP	β-tricalcium phosphate

ACKNOWLEDGMENTS

The authors want to acknowledge the financial support that allowed us to conduct a part of the experiments described within this paper: National Science Centre, Poland, a project entitled: *Investigation and modeling of the polymer solution cone formation in solution blow spinning process*. National Science Centre/Preludium/2014/13/N/ST8/01690.

REFERENCES

Abdal-hay A., Hamdy A.S., Khalil K.A., Lim J.H., 2015. A novel simple one-step air jet spinning approach for deposition of poly(vinyl acetate)/hydroxyapatite composite nanofibers on Ti implants. *Mater. Sci. Eng., C*, 49, 681–690. DOI: 10.1016/j.msec.2015.01.008.

Abdal-hay A., Hasan A., Yu-Kyoung, Lee M.-H., Hamdy A. S., Khalil K.A., 2016. Biocorrosion behavior of biodegradable nanocomposite fibers coated layer-by-layer on AM50 magnesium implant. *Mater. Sci. Eng., C*, 58, 1232–1241. DOI: 10.1016/j.msec.2015.09.065.

Abdal-hay A., Sheikh F.A., Lim J.K., 2013. Air jet spinning of hydroxyapatite/poly(lactic acid) hybrid nanocomposite membrane mats for bone tissue engineering. *Colloids Surf., B*, 102, 635–643. DOI: 10.1016/j.colsurfb.2012.09.017.

Balakrishnan H., Hassan A., Imran M., Wahit M.U., 2012. Toughening of polylactic acid nanocomposites: A short review. *Polymer-Plastics Technol. Eng.*, 51, 175–192. DOI: 10.1080/03602559.2011.618329.

Behrens A.M., Casey B.J., Sikorski M.J., Wu K.L., Tutak W., Sandler A.D., Kofinas P., 2014. In situ deposition of PLGA nanofibers via solution blow spinning. *ACS Macro Lett.*, 3, 249–254. DOI: 10.1021/mz500049x.

Bonan R.F., Mota M.F., da Costa Farias R.M., Silva S.D., Bonan P.R.F., Diesel L., Menezes R.R., da Cruz Perez D.E., 2019. *In vitro* antimicrobial and anticancer properties of TiO_2 blow-spun nanofibers containing silver nanoparticles. *Mater. Sci. Eng., C,* 104, 109876. DOI: 10.1016/j.msec.2019.109876.

Carlsson L., Röstlund T., Albrektsson B., Albrektsson T., Brånemark P.-I., 1986. Osseointegration of titanium implants. *Acta Orthop. Scand.*, 57, 285–289. DOI: 10.3109/17453678608994393.

Civantos A., Martínez-Campos E., Ramos V., Elvira C., Gallardo A., Abarrategi A., 2017. Titanium coatings and surface modifications: Toward clinically useful bioactive implants. *ACS Biomater. Sci. Eng.*, 3, 1245–1261. DOI: 10.1021/acsbiomaterials.6b00604.

Costa R.G.F., Brichi G.S., Ribeiro C., Mattoso L.H.C., 2016. Nanocomposite fibers of poly(lactic acid)/titanium dioxide prepared by solution blow spinning. *Polym. Bull.*, 73, 2973–2985. DOI: 10.1007/s00289-016-1635-1.

Daristotle J.L., Behrens A.M., Sandler A.D. Kofinas P., 2016. A review of the fundamental principles and applications of solution blow spinning. *ACS Appl. Mater. Interfaces*, 8, 34951–34963. DOI: 10.1021/acsami.6b12994.

Deneff J.I., Walton K.S., 2019. Production of metal-organic framework-bearing polystyrene fibers by solution blow spinning. *Chem. Eng. Sci.,* 203, 220–227. DOI: 10.1016/j.ces.2019.03.012.

Ferreira T.P.M., Nepomuceno N.C., Medeiros E.L.G., Medeiros E.S., Sampaio F.C., Oliveira J.E., Oliveira M.P., Galvão L.S., Bulhões E.O., Santos A.S.F., 2019. Antimicrobial coatings based on poly(dimethyl siloxane) and silver nanoparticles by solution blow spraying. *Prog. Org. Coat.,* 133, 19–26. DOI: 10.1016/j.porgcoat.2019.04.032.

François S., Chakfé N., Durand B., Laroche G., 2009. A poly(l-lactic acid) nanofibre mesh scaffold for endothelial cells on vascular prostheses. *Acta Biomater.*, 5, 2418–2428. DOI: 10.1016/j.actbio.2009.03.013.

Gregory C.A., Gunn W.G., Peister A., Prockop D.J., 2004. An Alizarin red-based assay of mineralisation by adherent cells in culture: comparison with cetylpyridinium chloride extraction. *Anal. Biochem.*, 329, 77–84. DOI: 10.1016/j.ab.2004.02.002.

Huang Y., Song J., Yang C., Long Y., Wu H., 2019. Scalable manufacturing and applications of nanofibers. *Mater. Today,* 28, 98–113. DOI: 10.1016/j.mattod.2019.04.018.

Jang J.-H., Castano O., Kim H.-W., 2009. Electrospun materials as potential platforms for bone tissue engineering. *Adv. Drug Delivery Rev.*, 61, 1065–1083. DOI: 10.1016/j.addr.2009.07.008.

Kopeć K., Wojasiński M., Ciach T., 2020. Superhydrophilic polyurethane/polydopamine nanofibrous materials enhancing cell adhesion for application in tissue engineering. *Int. J. Mol. Sci.*, 21, 6798. DOI: 10.3390/ijms21186798.

Latocha J., Wojasiński M., Jurczak K., Gierlotka S., Sobieszuk P., Ciach T., 2018. Precipitation of hydroxyapatite nanoparticles in 3D-printed reactors. *Chem. Eng. Process. Process Intensif.*, 133, 221–233. DOI: 10.1016/j.cep.2018.10.001.

Lewis R.J., Sr (Ed.), 1997. *Hawley's Condensed chemical dictionary*. 13th edition. John Wiley & Sons, Inc., New York, NY, p. 88.

Li J.P., Habibovic P., van den Doel M., Wilson C.E., de Wijn J.R., van Blitterswijk C.A., de Groot K., 2007. Bone ingrowth in porous titanium implants produced by 3D fiber deposition. *Biomaterials*, 28, 2810–2820. DOI: 10.1016/j.biomaterials.2007.02.020.

McEvoy G.K. (Ed.), 1992. *American hospital formulary service – Drug information 92*. American Society of Hospital Pharmacists, Inc., Bethesda, MD (Plus Supplements 1992), 276.

Medeiros E.L.G., Gomes D.S., Santos A.M.C., Vieira R.H., de Lima I.L., Rocha F.S., de S. Castro-Filice L., Medeiros E.S., Neves G.A., Menezes R.R., 2021. 3D nanofibrous bioactive glass scaffolds produced by one-step spinning process. *Ceram. Int.*, 47, 102–110. DOI: 10.1016/j.ceramint.2020.08.112.

Medeiros E.S., Glenn G.M., Klamczynski A.P., Orts W.J., Mattoso L.H.C., 2009. Solution blow spinning: A new method to produce micro- and nanofibers from polymer solutions. *J. Appl. Polym. Sci*. 113, 2322–2330. DOI: 10.1002/app.30275.

Ravichandran R., Ng C.C., Liao S., Pliszka D., Raghunath M., Ramakrishna S., Chan C.K., 2012. Biomimetic surface modification of titanium surfaces for early cell capture by advanced electrospinning. *Biomed. Mater.,* 7, 015001. DOI: 10.1088/1748-6041/7/1/015001.

Reneker D.H., Yarin A.L., 2008. Electrospinning jets and polymer nanofibers. *Polymer*, 49, 2387–2425. DOI: 10.1016/j.polymer.2008.02.002.

Roseti L., Parisi V., Petretta M., Cavallo C., Desando G., Bartolotti I., Grigolo B., 2017. Scaffolds for bone tissue engineering: State of the art and new perspectives. *Mater. Sci. Eng., C*, 78, 1246–1262. DOI: 10.1016/j.msec.2017.05.017.

Schindelin J., Arganda-Carreras I., Frise E., Kaynig V., Longair M., Pietzsch T., Preibisch S., Rueden C., Saalfeld S., Schmid B., Tinevez J.-Y., White D.J., Hartenstein V., Eliceiri K., Tomancak P., Cardona A., 2012. Fiji: an open-source platform for biological-image analysis. *Nat. Methods*, 9, 676–682. DOI: 10.1038/nmeth.2019.

Sharma B., Elisseeff J.H., 2004. Engineering structurally organised cartilage and bone tissues. *Ann. Biomed. Eng.*, 32, 148–159. DOI: 10.1023/b:abme.0000007799.60142.78.

Tammaro L., Vittoria V., Wyrwa R., Weisser J., Beer B., Thein S., Schnabelrauch M., 2014. Fabrication and characterisation of electrospun polylactide/β-tricalcium phosphate hybrid meshes for potential applications in hard tissue repair. *BioNanoMaterials*, 15, 9–20. DOI: 10.1515/bnm-2014-0001.

Tomecka E., Wojasinski M., Jastrzebska E., Chudy M., Ciach T., Brzozka Z., 2017. Poly(L-lactic acid) and polyurethane nanofibers fabricated by solution blow spinning as potential substrates for cardiac cell culture. *Mater. Sci. Eng., C*, 75, 305–316. DOI: 10.1016/j.msec.2017.02.055.

Tutak W., Sarkar S., Lin-Gibson S., Farooque T.M., Jyotsnendu G., Wang D., Kohn J., Bolikal D., Simon C.G., 2013. The support of bone marrow stromal cell differentiation by airbrushed nanofiber scaffolds. *Biomaterials*, 34, 2389–2398. DOI: 10.1016/j.biomaterials.2012.12.020.

Wojasiński M., Pilarek M., Ciach T., 2014. Comparative studies of electrospinning and solution blow spinning processes for the production of nanofibrous poly(L-lactic acid) materials for biomedical engineering. *Pol. J. Chem. Technol.*, 16, 43–50. DOI: 10.2478/pjct-2014-0028.

Zhang L., Kopperstad P., West M., Hedin N., Fong H., 2009. Generation of polymer ultrafine fibers through solution (air-) blowing. *J. Appl. Polym. Sci.*, 114, 3479–3486. DOI: 10.1002/app.30938.

Received 11 June 2021
Received in revised form 21 July 2021
Accepted 27 July 2021